Equilibrium and stability of axisymmetric drops on a conical substrate under gravity

A.K. Nurse, S. Colbert-Kelly, S.R. Coriell, and G. B. McFadden

National Institute of Standards and Technology

Gaithersburg, MD 20899

(Dated: April 8, 2015)

Motivated by recent investigations of toroidal tissue clusters that are observed to climb conical obstacles after self-assembly [Nurse et al., Journal of Applied Mechanics 79 (2012) 051013], we study a related problem of the determination of the equilibrium and stability of axisymmetric drops on a conical substrate in the presence of gravity. A variational principle is used to characterize equilibrium shapes that minimize surface energy and gravitational potential energy subject to a volume constraint, and the resulting Euler equation is solved numerically using an angle/arclength formulation. The resulting equilibria satisfy a Laplace-Young boundary condition that specifies the contact angle at the three-phase trijunction. The vertical position of the equilibrium drops on the cone is found to vary significantly with the dimensionless Bond number that represents the ratio of gravitational and capillary forces; a global force balance is used to examine the conditions that affect the drop positions. In particular, depending on the contact angle and the cone half-angle, we find that the vertical position of the drop can either increase ("the drop climbs the cone") or decrease due to a nominal increase in the gravitational force. Most of the equilibria correspond to upward-facing cones, and are analogous to sessile drops resting on a planar surface; however we also find equilibria that correspond to downward facing cones, that are instead analogous to pendant drops suspended vertically from a planar surface. The linear stability of the drops is determined by solving the eigenvalue problem associated with the second variation of the energy functional. The drops with positive Bond number are generally found to be unstable to non-axisymmetric perturbations that promote a tilting of the drop. Additional points of marginal stability are found that correspond to limit points of the axisymmetric base state. Drops that are far from the tip are subject to azimuthal instabilities with higher mode numbers that are analogous to the Rayleigh instability of a cylindrical interface. We have also found a range of completely stable solutions that correspond to small contact angles and cone half-angles.

I. INTRODUCTION

Capillary forces lead to a rich collection of problems in physics, chemistry, and materials science that have both beauty and technological importance [1]. Shapes such as soap films, drops, and bubbles display interesting dynamical and equilibrium behavior, and have been studied in a variety of settings (see, e.g. the review articles [2–5] and references therein). Here we study the equilibrium and stability of an axisymmetric liquid drop that is resting on the side of a conical solid substrate under the combined effects of capillarity and gravity. This study is motivated by recent experimental observations of the behavior of clusters of biological cells that self-assemble at the bottom of patterned containers [6, 7]. Each compartment of the partitioned container includes a conical obstruction in its base that interrupts the tissue assembly, leading to toroidal clusters of cells at the base of each cone. After assembly, a cell cluster is often observed to climb up the side of the cone. A possible mechanism for this dynamical behavior is based on the interplay of capillarity and gravitational forces: a toroidal tissue cluster would like to reduce its surface area, which it can do by reducing its major radius (the long way around the torus) by moving to higher positions on the cone. In climbing the cone the gravitational potential energy of the sample is increased, so the dynamical process must balance both forms of energy. A model of the dynamical process based on toroidally-shaped clusters evolving by surface diffusion has been used to interpret the experimental observations, which occasionally included both tilting of the cell cluster relative to the cone axis, and the development of fluted distortions in the azimuthal direction.

In the light of these interesting experiments it seems desirable to consider the simpler problem of determining the equilibrium and stability of liquid drops on a conical substrate. As in previous studies [8] of liquid equilibrium and stability in cylindrical geometries that arise in material processing applications, we formulate a variational statement of the problem in terms of an energy functional containing both surface energy and gravitational potential energy contributions subject to a volume constraint. For simplicity we ignore any effects of surface roughness, and assume that there is no resistance to lateral motion of the drop along the surface of the cone (no contact angle hysteresis). Axisymmetric stationary shapes that extremize the energy then satisfy the Laplace-Young equation that represents the local balance of capillary, gravitational, and pressure forces at each point of the interface. Appropriate natural boundary conditions at the contact line where the drop, substrate, and surrounding fluid meet also follow from the variational principle, yielding the familiar Young boundary condition that determines the drop's contact angle at the trijunction. The second variation of the energy functional is examined numerically to determine the linear stability

of the equilibrium shapes. Since the surface energies and resulting contact angles in the above experiments have not been directly measured, we present results for a range of conditions and material properties.

The present work is related to a number of previous studies. Experimentally, macroscopic liquid toroidal droplets [9] and nanoscale toroids of varying sizes have been carefully generated and observed [10, 11]. Analysis indicates that the stability of these toroidal shapes is related to the aspect ratio of the major and minor radii. Bostwick and Steen [12] consider the stability of constrained cylindrical fluid interfaces, including a treatment of the equilibrium and stability of toroidal surfaces that are partially supported by a cylindrical cup-like solid. González, Diez, and Kondic [13] study the equilibrium and stability of a liquid ring on a horizontal substrate via a long-wave theory, including a linear stability analysis of the dynamic equations and a numerical solution that includes nonlinear effects leading to droplet breakup. A number of authors have discussed the dynamic instability of isolated toroidal drops based on approximate base states that are assumed to have circular cross sections [14, 15], or have observed or simulated the temporal evolution of arbitrary (non-equilibrium) toroidal shapes [11, 16–18].

Our approach focuses on the accurate computation of bifurcation points for self-consistent equilibrium shapes on a conical substrate that are computed from a variational principle. In the next section we describe the model and formulate the variational principle. In §III we describe the Euler equation and boundary conditions for the axisymmetric equilibrium shapes, and outline the numerical procedure for their computation. In §IV we describe the axisymmetric equilibrium shapes, including a quantitative discussion of the overall forces balance on the drop. In §V we consider the stability of the axisymmetric drops to both axisymmetric and non-axisymmetric disturbances, followed by a discussion in §VI.

II. MODEL

We consider the equilibrium and stability of an axisymmetric liquid drop lying on the surface of a cone. The drop is surrounded by a passive external liquid or vapor; for notational convenience, we will refer to the surrounding fluid as vapor. The cone surface is assumed to be smooth and defect-free, so that the three-phase contact line can move without resistance in determining the shape and location of an equilibrium drop. In a cylindrical coordinate system (r, θ, z) with origin at the apex of the cone, the surface of the cone is assumed to be given by $r = -z \tan \beta$ for $z_L < z < 0$, where β is the half-angle of the apex of the cone and $-z_L$ is the total height of the cone, taken to be large enough that it does not interfere with the drop shape (see Fig. 1). The gravitational field $-g\hat{z}$ is aligned with the axis of the cone, where $\hat{z}$ is a unit vector in the positive z direction. We recall that the lateral surface area and volume of a cone of height H and base radius R are given by $S = \pi R \sqrt{R^2 + H^2}$ and $V = \pi R^2 H/3$.

We first formulate a variational statement for the equilibrium shape assuming that the the axisymmetric drop has a single-valued representation $r = f(z)$; we will subsequently convert to a more general angle-arclength formulation.

A. Variational Principle for Axisymmetric Drops

A variational approach states that the shape is an extremal of the constrained Lagrangian functional

$$\mathcal{L} = E_S + E_G - P V_D, \tag{1}$$

where E_S represents the total surface energy of the system, E_G represents the gravitational potential energy of the drop, V_D is the drop volume, and P is a Lagrange multiplier utilized to enforce the volume constraint $V_D = \text{constant}$. We assume the drop extends over the range $z_1 < z < z_0 < 0$; the endpoints z_0 and z_1 are unknowns that must be determined as part of the solution. The total surface energy of the system is given by

$$E_S = E_{LV} + E_{SL} + E_{SV}, \tag{2}$$

where

$$E_{LV} = 2\pi \gamma_{LV} \int_{z_1}^{z_0} f(z) \sqrt{1 + f_z^2} \, dz \tag{3}$$

is the surface energy of the drop in contact with vapor,

$$E_{SL} = \pi \gamma_{SL} \left[r_1 \sqrt{r_1^2 + z_1^2} - r_0 \sqrt{r_0^2 + z_0^2} \right] \tag{4}$$
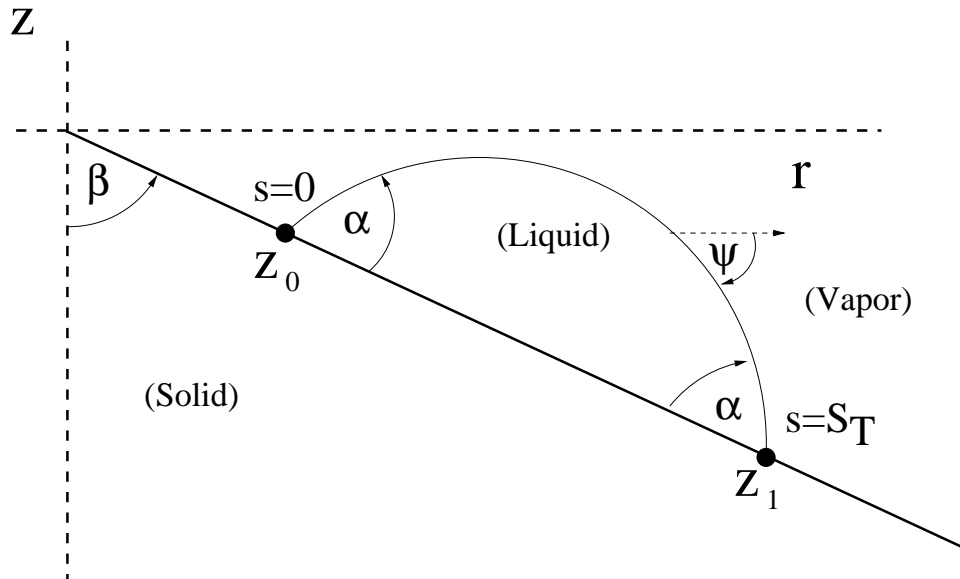
FIG. 1: Schematic of a liquid drop on a conical solid with half-angle β. The drop has contact lines at $z = z_0$ and $z = z_1$ where the contact angle is α. The arclength of the drop varies from $s = 0$ at $z = z_0$ to $s = S_T$ at $z = z_1$, and the tangent to the drop makes an angle ψ with respect to the horizontal.

is the surface energy of the drop in contact with the cone, and

$$E_{SV} = \pi \gamma_{SV} \left[r_L \sqrt{r_L^2 + z_L^2} - r_1 \sqrt{r_1^2 + z_1^2} + r_0 \sqrt{r_0^2 + z_0^2} \right] \tag{5}$$

is the surface energy of the cone that is exposed to vapor. Here the liquid-vapor surface energy γ_{LV}, the solid-liquid surface energy γ_{SL}, and the solid-vapor surface energy γ_{SV} are assumed to be constant, and $r_0 = -z_0 \tan \beta$, $r_1 = -z_1 \tan \beta$, and $r_L = -z_L \tan \beta$ are the radii at heights z_0, z_1, and z_L, respectively. The volume of the drop V_D is given by

$$V_D = V_T - V_C, \tag{6}$$

where

$$V_T = \pi \int_{z_1}^{z_0} [f(z)]^2 \, dz \tag{7}$$

is the total volume of the drop plus that of the underlying portion of the cone between z_1 and z_0; the latter is

$$V_C = \frac{\pi}{3} \left[r_0^2 z_0 - r_1^2 z_1 \right]. \tag{8}$$

Similarly, the potential energy of the drop E_G is given by

$$E_G = \pi \Delta \rho g \left\{ \int_{z_1}^{z_0} z [f(z)]^2 \, dz - \frac{1}{4} [z_1^2 r_1^2 - z_0^2 r_0^2] \right\}, \tag{9}$$

where $\Delta \rho = (\rho_L - \rho_V)$ is the (constant) density difference between the liquid and vapor, and g is the gravitational acceleration. The integral term includes contributions from both the liquid drop and the solid cone, and the latter term removes the solid contribution.

III. EQUILIBRIUM SHAPE

A. Euler Equation and Boundary Conditions

The surface shape $f(z)$ and the points $z = z_0$ and $z = z_1$ are coupled through the relations

$$f(z_0) + z_0 \tan \beta = 0, \quad f(z_1) + z_1 \tan \beta = 0, \tag{10}$$

stating that z_0 and z_1 represent a contact line of the three-phase system. Requiring the functional to be stationary with respect to variations δf yields the Euler equation

$$0 = \gamma_{LV} K + \Delta \rho \, g \, z - P, \tag{11}$$

where

$$K = \frac{1}{f \sqrt{1 + f_z^2}} - \frac{f_{zz}}{(1 + f_z^2)^{3/2}} \tag{12}$$

is the mean curvature of the liquid-vapor interface. Variations with respect to δz_0, and δz_1 that are consistent with the relations (10) then yield boundary conditions for the local slopes at the contact lines,

$$f_z(z_0) = \tan(\beta + \alpha), \quad f_z(z_1) = \tan(\beta - \alpha), \tag{13}$$

where the contact angle α is determined by the Young equation of interfacial energy balance

$$\gamma_{SV} = \gamma_{SL} + \gamma_{LV} \cos \alpha. \tag{14}$$

The Euler equation is equivalent to the local mechanical Laplace-Young equation $p_{\text{inner}} = p_{\text{outer}} + \gamma_{LV} K$ along the liquid-vapor interface, where the equilibrium vapor pressure $p_V = \bar{p}_V - \rho_V g z$ and the equilibrium liquid pressure $p_L = \bar{p}_L - \rho_L g z$ are hydrostatic, where $\bar{p}_V$ and $\bar{p}_L$ are constants; the Lagrange multiplier is then given by $P = \bar{p}_L - \bar{p}_V$. The Young equation given by Eq. (14) plays the role of a tangential balance of surface tensions at the contact line [19].

B.   Angle/Arclength Formulation

We next represent the drop in parametric form as $r = R(s)$ and $z = Z(s)$ where s is the local arclength of the curve, measured from z_0 to z_1. The local tangent angle $\psi(s)$ is defined by

$$\frac{dR}{ds} = \cos \psi, \quad \frac{dZ}{ds} = \sin \psi, \tag{15}$$

and the Euler equation takes the form of a first order ordinary differential equation (ODE) for ψ,

$$\gamma_{LV} \left[\frac{d\psi}{ds} + \frac{\sin \psi}{R} \right] = \Delta \rho g Z - P, \tag{16}$$

over an interval $0 < s < S_T$ of total arclength S_T. Here we have used the geometric relations

$$K = -\frac{d\psi}{ds} - \frac{\sin \psi}{R}, \quad \frac{1}{\sqrt{1 + f_z^2}} = -\sin \psi. \tag{17}$$

For a single-valued representation $r = f(z)$ the angle ψ is negative with our sign convention. However, the final angle/arclength equations can be applied to more general drop shapes that would correspond to a multi-valued $f(z)$. An equivalent alternative approach (see, e.g., [20]) is to reformulate the Lagrangian in terms of angle/arclength variables from the start and apply suitably constrained variations to obtain the Euler equations in angle/arclength form directly.

The specified drop volume is $V_D = V_T - V_C$, where the total volume V_T and the cone volume V_C are defined by

$$V_T = -\pi \int_0^{S_T} R^2 \, \sin \psi \, ds, \quad V_C = \frac{\pi}{3} \left[r_0^2 z_0 - r_1^2 z_1 \right]. \tag{18}$$

V_T can be determined by solving the additional ODE,

$$\frac{dV_T}{ds} = -\pi R^2 \sin \psi, \tag{19}$$

with the boundary condition $V_T(0) = 0$; we then set $V_D = V_T(S_T) - V_C$. The other boundary conditions take the form

$$Z(0) = z_0, \quad Z(S_T) = z_1, \tag{20}$$

$$R(0) = r_0 = -z_0 \tan \beta, \quad R(S_T) = r_1 = -z_1 \tan \beta, \tag{21}$$

$$\psi(0) = \beta + \alpha - \pi/2, \quad \psi(S_T) = \beta - \alpha - \pi/2. \tag{22}$$
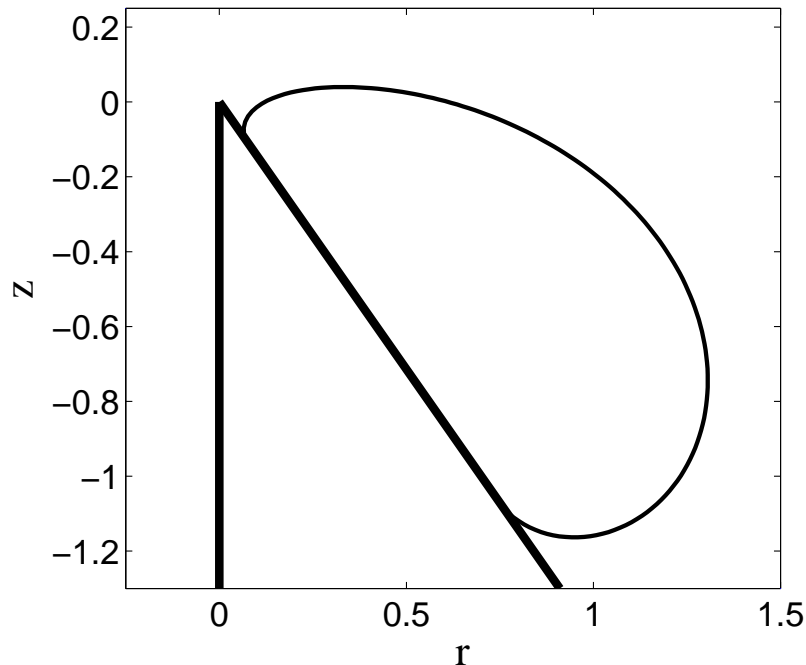
FIG. 2: Side view of the right hand half of an azimuthal cross section of the cone and drop for Bo = 1.85, $\alpha = 170^o$, and $\beta = 35^o$.

C. Numerical Procedure

A numerical technique for determining the equilibrium shape can be formulated via a shooting procedure [8], with the parameters z_0, z_1, P, and S_T considered as unknowns. The given data for the solution are the cone half angle β, the contact angle α, and the drop volume V_D. Since the total arclength of the solution is unknown in advance, we employ a normalized arclength variable $t = s/S_T$, which introduces an explicit dependence on S_T in the ODEs. Given provisional values for the variables z_0, P, and S_T, these ODEs are integrated from $t = 0$ to $t = 1$. Since the provisional values generally lead to incorrect values of the contact condition $R(S_T) + Z(S_T)\tan\beta = 0$, the slope $\psi_1 = \psi(S_T)$ at $z_1 = Z(S_T)$, and the drop volume V_D, the provisional values of z_0, P, and S_T are then adjusted iteratively so that these three remaining boundary conditions, $V_D = V_T - V_C$, $\psi_1 = \beta - \alpha - \pi/2$, and $r_1 + z_1 \tan\beta = 0$, are satisfied.

IV. EQUILIBRIUM RESULTS FOR AXISYMMETRIC DROPS

We define a length scale $\bar{R}$ based on the given drop volume V_D by setting $V_D = 4\pi\bar{R}^3/3$; that is, $\bar{R}$ is the radius of a sphere of equivalent volume. The ratio of gravitational and surface tension forces defines the Bond number Bo $= \Delta\rho g \bar{R}^2/\gamma_{LV}$. A representative water drop in air with diameter $2\bar{R} = 5.0 \cdot 10^{-3}$ m, density $\Delta\rho = 10^3$ Kg/m^3, surface energy $\gamma_{LV} = 75 \cdot 10^{-3}$ N/m, and gravitational acceleration $g = 9.8$ m/s^2 has Bo ≈ 0.8. Results are presented in dimensionless units based on the length scale $\bar{R}$, so that the corresponding dimensionless drop volume is $4\pi/3$.

A. Numerical Results

An example for a cone of half-angle $\beta = 35^o$ with Bond number Bo $= 1.85$ is shown in Fig. 2. Here the axisymmetric drop is shown in cross-section, and the cone axis and surface are the thick lines issuing from the cone apex at $r = 0$ and $z = 0$. The Bond number is large enough that the effects of gravity are apparent, with the drop sagging at its lower end. The drop partially wets the cone with a relatively large contact angle $\alpha = 170^o$, so that the drop would have a multi-valued representation $r = f(z)$.
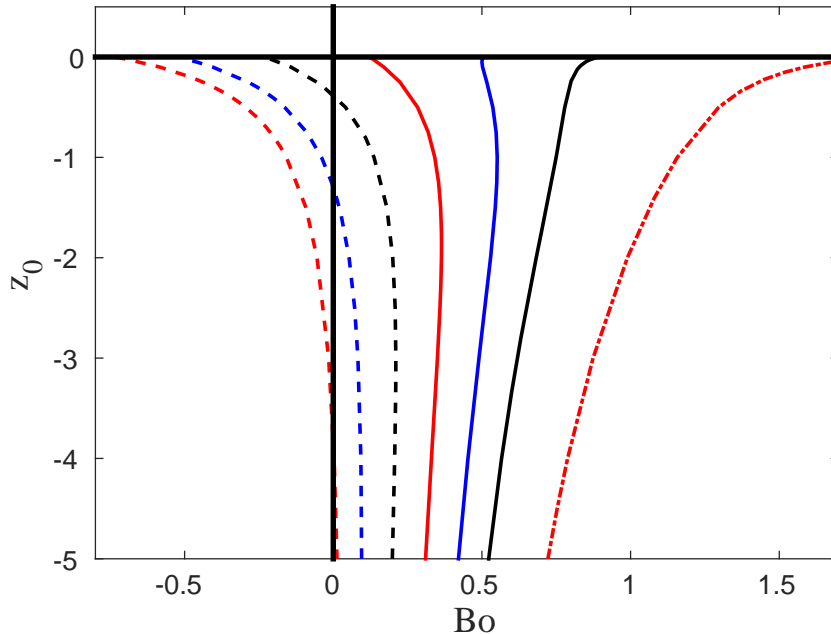
FIG. 3: Location of the upper contact line, z_0, versus the Bond number Bo for a conical half-angle of $\beta = 35^o$ for various values of the contact angle α. From left to right, the curves correspond to $\alpha = 15^o$ (red dashed), 30° (blue dashed), 45° (black dashed), 60° (red), 75° (blue), 90° (black), and 135° (red chain-dashed).

For given values of β and α, the upper and lower endpoint of the drop, z_0 and z_1, vary as the Bond number is changed. A summary of equilibrium calculations for a cone with half-angle $\beta = 35^o$ is shown in Fig. 3, where the location of the upper contact line $z = z_0$ is plotted versus Bo for various values of α. In all cases that we have considered both z_0 and z_1 vary in tandem with similarly-sized changes as the Bond number is varied; this behavior is not unexpected in view of the imposed volume constraint. We have chosen to plot z_0 rather than z_1 since z_0 gives a better indication of the drop's proximity to the tip. Note that the contact angle α is a material parameter, so that parametric variations in α correspond to a different choice of materials. We find that for drops with contact angles greater than 90° the equilibrium position of the drop moves up the cone with increasing Bond number. An example is shown in Fig. 4, where three drops having the same contact angles but differing values of Bo are shown. For drops with contact angles less than 90° the situation is more complicated, as the equilibrium position of the drop can vary non-monotonically with Bond number. An example where the drop moves down the cone with increasing Bond number is shown in Fig. 5.

It is perhaps surprising that an increase in the effect of gravity can cause the equilibrium position of a drop to rise on the cone. Although the expected dynamic response of a drop to an increase in gravity would be a shift to positions lower on the cone, all other effects being equal, here we are considering the different question of how the drop's *equilibrium* position varies with an increase in gravity. In that case, the drop shifts in the direction required to strengthen the compensating forces that are in equilibrium with the gravitational force. Depending on the detailed behavior of these other forces, this may require a change in position either up or down the cone, as illustrated in Fig. 4 and Fig. 5. In §IV C below we return to the question of the net balance between gravitational and capillary forces to help interpret these results in a more quantitative fashion.

We note that in Fig. 3 not only are there curves with both positive and negative slope, but the curves corresponding to smaller contact angles can have equilibria corresponding to zero Bond numbers and even negative Bond numbers. Equilibria for zero Bond number are indeed possible for appropriate values of α and β, as will be discussed in §IV B below. Solutions corresponding to a negative Bond number need to be re-interpreted in terms of the definition $\text{Bo} = \Delta\rho g \bar{R}^2/\gamma_{LV}$: they correspond either to a lighter drop in a heavier fluid ($\Delta\rho < 0$), or to a inverted geometry with the cone pointing downward rather than upward. An examination (not shown) of the drops with Bo < 0 shows that they bulge upward rather than downward in contrast to the Bo > 0 result in Fig. 2.

The non-monotonic regions of the curves support multiple equilibrium solutions for the same values of β, α, and Bo; an example is shown in Fig. 6. We emphasize that these shapes correspond to stationary points of the energy,
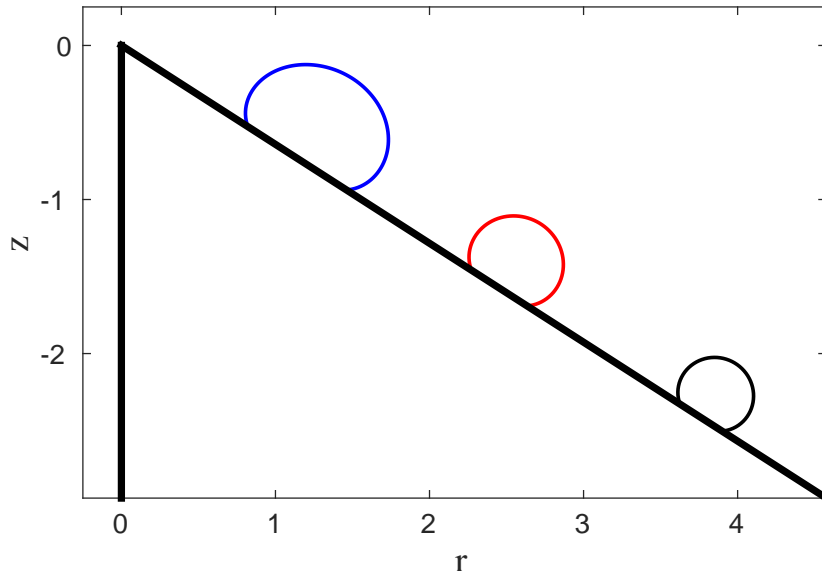
FIG. 4: Three equilibrium drops with contact angle $\alpha = 143^o$ on a cone with half-angle $\beta = 57^o$. From top to bottom, the corresponding Bond numbers are Bo = 2.5 (blue), 1.9 (red), and 1.6 (black), respectively.

and one or both of them could correspond to an unstable equilibrium. We will address the stability of the equilibrium shapes by examining the second variation of the energy functional in §V below. We note that the curve for $\alpha = 75^o$ in Fig. 3 actually exhibits two inflection points, one very near the apex of the cone (small $|z_0|$), as will be discussed in more detail in §V C when we consider the stability of these equilibria.

In Fig. 7 we summarize the existence of equilibria with various cone half-angles β for a given contact angle $\alpha = 75^o$. The overall trends are similar to those shown in Fig. 3, with larger values of β producing monotonic curves with positive slope corresponding to drops that are higher on the cone for increasing Bond numbers. For moderate cone angles the curves may again be non-monotonic, and zero and negative Bond numbers can be obtained. For very small values of β the cone has a near-vertical slope, and the height of the drop on the cone becomes very sensitive to Bond number: small changes in Bo produce large excursions in the equilibrium drop position.

B. Zero Bond Number Solutions

For zero Bond number the Euler equation reduces to the condition that the mean curvature of the drop is constant. An exact solution in this case corresponds to a portion of a sphere: namely, a sphere that is "punctured" by a given cone so that the cone axis lies along a diameter of the sphere, with the tip of the cone protruding outside the sphere. In our coordinate system, if the center of the sphere is located at $r = 0$ and $z = z_c < 0$, then the spherical surface outside the cone represents a valid solution if the radius of the sphere R_c lies in the range $|z_c| > R_c > |z_c| \sin \beta$. For $R_c = |z_c|$ the drop just touches the tip of the cone with a contact angle $\alpha = \pi/2 - \beta$, and for $R_c = |z_c| \sin \beta$ the sphere lies entirely inside the cone making tangential contact with the cone ($\alpha = 0$) at the height $-|z_c| \cos^2 \beta$. The azimuthal cross section of the resulting drop is symmetric about the diameter of the sphere that bisects the chord from $|z_0|$ to $|z_1|$, so that the corresponding contact angles at z_0 and z_1 are equal. As parameterized by R_c, the resulting volume of the drop and the contact angles vary monotonically with R_c. Since the cone geometry is scale invariant, a drop with the desired volume can be obtained by a change in the overall length scale, which does not affect the contact angle.

As an aside, for the related problem of determining the equilibrium shape of an axisymmetric drop lying on the
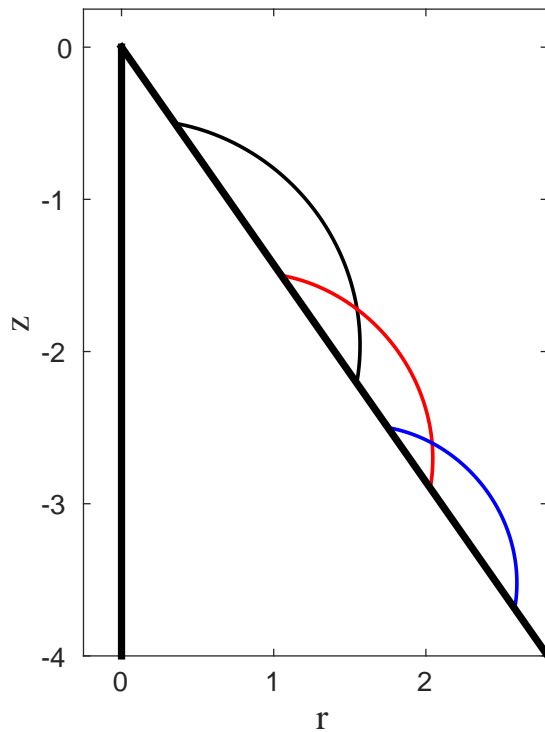
FIG. 5: Three equilibrium drops with contact angle $\alpha = 45^o$ on a cone with half-angle $\beta = 35^o$. From top to bottom, the corresponding Bond numbers are Bo = 0.041 (black), 0.180 (red), and 0.208 (blue), respectively.

surface of a cylinder in zero gravity, there are also analytical solutions corresponding to portions of a sphere, in this case a sphere that is punctured by the cylinder. The spherical geometry in this case restricts the resulting contact angles to values less than 90°. However, non-spherical solutions with constant curvature are also possible; for example, solutions with contact angles larger than 90° can readily be computed (see Fig. 8). We have searched unsuccessfully for non-spherical numerical solutions with zero Bond number for the conical problem. The Bo = 0 solutions in Fig. 3 for contact angles in the range $\alpha < \pi/2 - \beta$ are all found to correspond to portions of a sphere. For $\alpha > \pi/2 - \beta$ we find no Bo = 0 solutions.

C. Balance of Gravitational and Capillary Forces

Although the Young equation (14) represents an energy balance, it is useful to also interpret it as a local tangential force balance. For example, at the upper contact line at $z = z_0$ the solid-vapor interface effectively exerts a tangential force with an upward component, the solid-liquid interface exerts a tangential force with a downward component, and the tangential force component of the liquid-vapor interface is downward for $\alpha < \pi/2$ and and upward for $\alpha > \pi/2$. The reverse behavior holds at the lower contact line at $z = z_1$. Similarly, the Laplace-Young equation (11) represents a local balance of pressure and capillary forces at each point of the liquid-vapor interface. In this section we consider an integral force balance on the entire drop rather than these local balances. In particular, we seek the form of the vertical force on the drop that must balance the gravitational force $F_g = -(\rho_L V_D)g\hat{z}$ under equilibrium conditions.
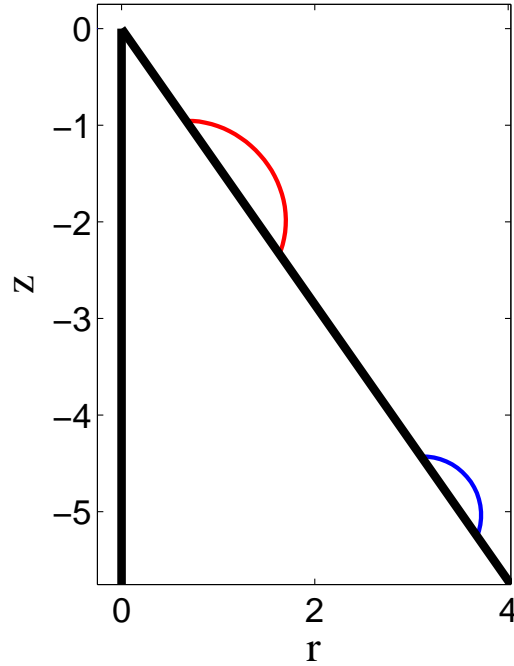
FIG. 6: Two equilibrium drops with contact angle $\alpha = 57.3^o$ on a cone with half-angle $\beta = 35^o$. The Bond number for both is Bo = 0.3, and the drops represent different solutions under identical conditions.

1. Derivation in Cartesian Coordinates

We first integrate the steady-state volumetric force balance $\nabla p = -\rho_L g \hat{z}$ over the volume of the drop Ω_D, and use the divergence theorem to obtain the expression

$$\int_{S_D} p_L \, \hat{n} \, dA = -\hat{z} \int_{\Omega_D} \rho_L \, g \, dV = -\rho_L g V_D \hat{z}, \tag{23}$$

where S_D is the surface of the drop, consisting of the solid-liquid interface S_{SL} and the liquid-vapor interface S_{LV}, $\hat{n}$ is the outward normal to S_D, and dV and dA are the volume and surface differentials. We assume the drop is expressed in the single-valued form $r = f(z)$. Evaluating the vertical component of the integral over the surface of the cone with the hydrostatic pressure field $p_L = \bar{P}_L - \rho_L g z$, where $\bar{P}_L$ is constant, gives

$$\int_{S_{SL}} p_L \, \hat{n} \cdot \hat{z} \, dA = \bar{P}_L \pi (r_0^2 - r_1^2) - 2\rho_L g V_C, \tag{24}$$

where $V_C = \pi(z_0 r_0^2 - z_1 r_1^2)/3$ is the volume of the conical section from z_0 to z_1. Next evaluating the integral over the liquid-vapor interface with the hydrostatic pressure field $p_L = p_V + \gamma_{LV} K = \bar{P}_V - \rho_V g z + \gamma_{LV} K$, where $\bar{P}_V$ is constant, gives

$$\int_{S_{VL}} p_L \, \hat{n} \cdot \hat{z} \, dA = -\bar{P}_V \pi (r_0^2 - r_1^2) + \rho_V g(2V_C - V_D) - 2\pi \gamma_{LV} \left\{ \frac{r_0}{\sqrt{1 + [f_z(z_0)]^2}} - \frac{r_1}{\sqrt{1 + [f_z(z_1)]^2}} \right\}. \tag{25}$$

Combining these expressions gives the result

$$-[\rho_L - \rho_V]g V_D = [\bar{P}_L - \bar{P}_V]\pi(r_0^2 - r_1^2) - 2[\rho_L - \rho_V]g V_C - 2\pi \gamma_{LV} \left\{ \frac{r_0}{\sqrt{1 + [f_z(z_0)]^2}} - \frac{r_1}{\sqrt{1 + [f_z(z_1)]^2}} \right\}. \tag{26}$$

We discuss the terms in this expression in more detail in the following subsection.
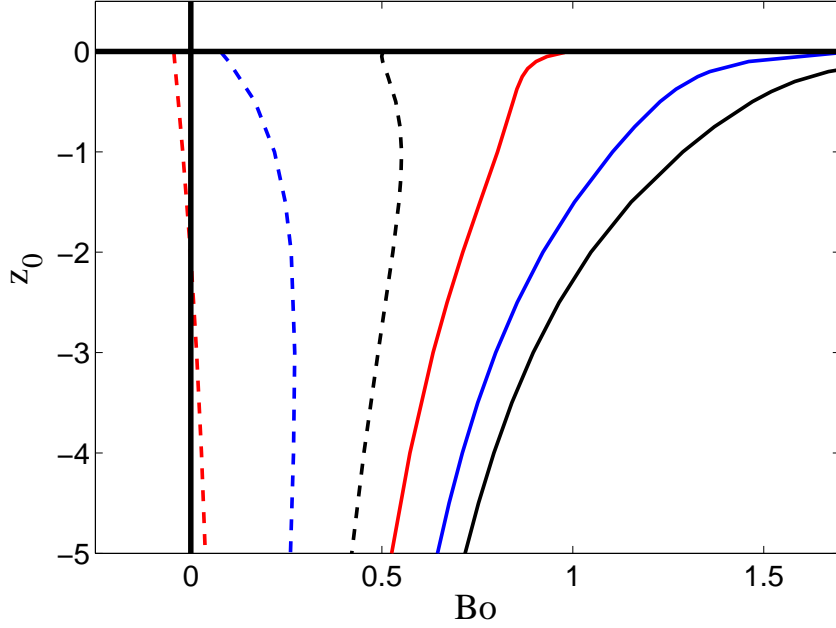
FIG. 7: Location of the upper contact line, z_0, versus the Bond number Bo for drops with a contact angle $\alpha = 75^o$ for various values of the conical half-angle β. From left to right, the curves correspond to $\beta = 5^o$ (red dashed), 20° (blue dashed), 35° (black dashed), 45° (red), 55° (blue), and 60° (black).

2. Derivation in Angle/Arclength Coordinates

The force balance in Eq. (26) can also be derived directly from the Euler equation (16), although the above derivation in Cartesian coordinates helps to interpret the origin of the various forces. Multiplying Eq. (16) by $R_s = \cos\psi$ produces the identity

$$\gamma_{LV}[R\sin\psi]_s + \frac{P}{2}[R^2]_s - \frac{\Delta\rho\, g}{2}Z[R^2]_s = 0. \tag{27}$$

Integrating from $s = 0$ to $s = S_T$ followed by an integration by parts leads to the expression

$$0 = -[\rho_L - \rho_V]\, g\, V_D + 2[\rho_L - \rho_V]\, g\, V_C + P\pi(r_1^2 - r_0^2) - 2\pi\gamma_{LV}r_0\sin\psi_0 + 2\pi\gamma_{LV}r_1\sin\psi_1 \tag{28}$$

$$= F^B + F_c^B + F^P + F_0^C + F_1^C,$$

which generalizes Eq. (26) to include the case of multi-valued interfaces. We have introduced the notation

$$F^B = -[\rho_L - \rho_V]\, g\, V_D, \quad F_c^B = 2\,[\rho_L - \rho_V]\, g\, V_C, \quad F^P = P\pi(r_1^2 - r_0^2), \tag{29}$$

$$F_0^C = -2\pi\gamma_{LV}r_0\sin\psi_0, \quad F_1^C = 2\pi\gamma_{LV}r_1\sin\psi_1, \tag{30}$$

so that the conditions of a vertical force balance on the drop is that the sum of these five terms must vanish, with the sign convention that a positive term corresponds to an upwards force. The effective gravitational force on the drop is F^B, as corrected by the effects of the contacting vapor; for example, according to Archimedes principle $[\rho_L - \rho_V]\, g\, V_D$ would be the net buoyancy force on the drop if it were completely surrounded by vapor. There is also a net force resulting from contact with the cone, represented by F_c^B. F^P represents an effective constraint force proportional to the Lagrange multiplier P that imposes the condition of constant drop volume. F_0^C and F_1^C are the capillary forces at the contact lines at z_0 and z_1. The capillary forces depend on $\sin\psi_0$ and $\sin\psi_1$, where ψ_0 and ψ_1 are the angles that the liquid-vapor interface make at the contact lines with respect to the horizontal. These angles, in turn, are determined by the contact angle α and cone half-angle β through Eq. (22). The capillary forces can either oppose or reinforce each other, depending on the specific values of α and β.
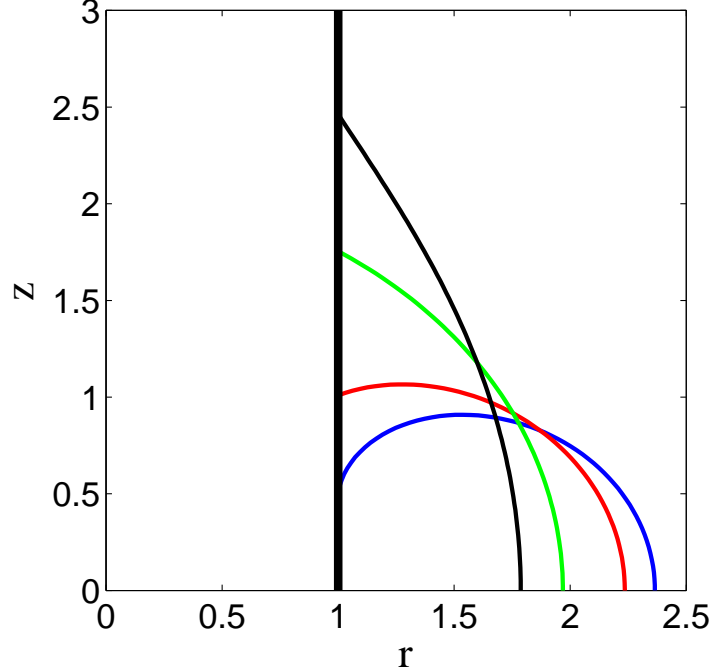
FIG. 8: Cross section of the upper half ($z > 0$) of equilibrium drops of equal volume on the side of a cylinder of unit radius in zero gravity (Bo $= 0$). The contact angles are $\alpha = 28.6^o$ (black), 57.3^o (green), 114.6^o, and 171.9^o .

3. Force Balance for Zero Bond Number

The force balance simplifies in the case of zero Bond number, since F^B and F_c^B both vanish for $g = 0$. For the Bo $= 0$ case with $\beta = 35^o$, the remaining terms F^P, F_0^C, and F_1^C are plotted versus the contact angle α in Fig. 9. For α tending to $\pi/2 - \beta = 55^o$ the upper contact line at z_0 approaches the cone tip. For the indicated range of α both ψ_0 and ψ_1 are between $-\pi/2$ and zero, and $\sin\psi_0$ and $\sin\psi_1$ are both negative. The capillary forces are in opposite directions, with the upper contact line pulling the drop upwards and the lower contact line pulling it downwards. The capillary force F_1^C at z_1, which scales with r_1, dominates F_0^C, which scales with r_0, in magnitude; F_0^C becomes negligible as the drop approaches the tip of the cone. The net capillary forces balance the force F^P, which is upwards along this solution branch; for drops with a spherical surface the Lagrange multiplier is positive, $P = 2/R_c > 0$. Note that for a spherical surface, the principle curvatures $-d\psi/ds$ and $-\sin\psi/R$ are constant and equal, and the Euler equation (16) with $g = 0$ can be written as

$$2\pi R \sin\psi\, \gamma_{LV} + \pi R^2\, P = 0, \tag{31}$$

which represents a local balance between capillary and constraint forces at each point.

4. Force Balance for Non-Zero Bond Numbers

We next describe some force balance results for non-zero Bond numbers. We let $F_T^P = F_c^B + F^P$ represent the combined forces of the cone exerted on the drop, so that the net force balance is $F_0^C + F_1^C + F^B + F_T^P = 0$.

In Fig. 10 we show components of the force balance for the case $\alpha = 135^o$ and $\beta = 35^o$. The drop climbs the cone with increasing Bond number in this case (see Fig. 3), and the surface slopes at the contact lines satisfy $\sin\psi_0 = 0.98$ and $\sin\psi_1 = 0.17$. The capillary forces at the contact lines are therefore in opposite directions, with F_0^C tending to dominate F_1^C (except near the tip). The buoyancy force F^B and the net capillary force $F^C = F_1^C + F_0^C$ are both negative (downward) in this case, and are balanced by the positive (upward) supporting force F_T^P provided by the cone. The magnitude of the buoyancy force increases slightly for higher drops, while the capillary forces weaken with height, as does the net force from the cone.
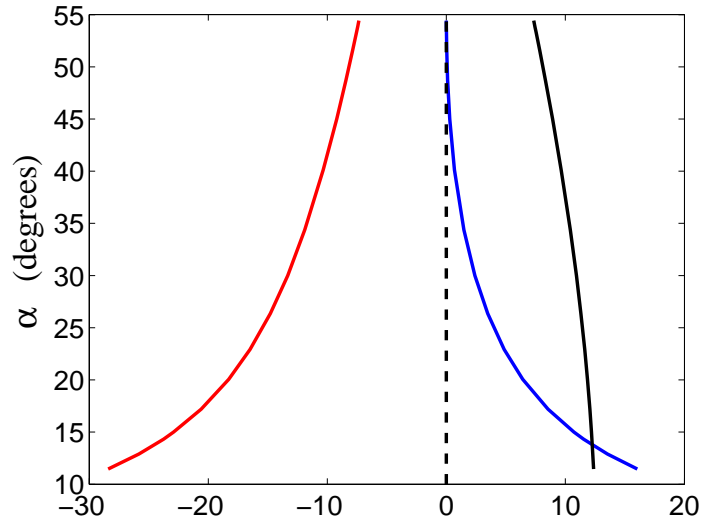
FIG. 9: Vertical force balance between the capillary forces F_0^C (blue curve) and F_1^C (red curve) at z_0 and z_1, and the effective constraint force due to the cone, F^P (black curve), with Bo $= 0$ and $\beta = 35^o$ for various contact angles α (vertical axis); these forces (shown on the horizontal axis) sum to zero.

In Fig. 11 we show components of the force balance for the case $\alpha = 60^o$ and $\beta = 35^o$. In this case the Bond number initially increases with height, but reaches a limit point at a height $z_0 \approx -1.9$, and then decreases with further increases in z_0, although the Bond number never becomes negative (see Fig. 3). The surface slopes at the contact lines satisfy $\sin \psi_0 = 0.09$ and $\sin \psi_1 = -0.9$, and the capillary forces are therefore in the same direction, but with F_1^C now dominating F_0^C in magnitude. The overall balance is between the upward net force from the cone and the downward capillary force F_1^C at the lower contact line; the resulting buoyancy force on the drop is relatively small.

In Fig. 12 we show components of the force balance for the case $\alpha = 30^o$ and $\beta = 35^o$. In this case the Bond number is initially positive and decreasing with height, passing through zero at a height $z_0 \approx -1.29$, and then remaining negative for higher drops. The surface slopes at the contact lines satisfy $\sin \psi_0 = -0.42$ and $\sin \psi_1 = -0.996$, and the capillary forces are therefore in opposite directions, with F_1^C tending to dominate F_0^C in magnitude. The overall balance is between the upward net force provided by the cone and the upper contact line and the downward force at the lower contact line; the resulting buoyancy force on the drop is relatively small, and reverses direction from downward to upward at $z_0 \approx -1.29$.

V. SECOND VARIATION AND STABILITY

To assess the stability of the solutions we proceed to consider the second variation of the energy functional. For a single-valued interface, this entails generalizing the shape to a non-axisymmetric representation $r = f(z, \theta)$ with contact lines $z = z_0(\theta)$ and $z = z_1(\theta)$. The appropriate expressions for E_S, E_G and V_D in Eq. (1) are then varied as before to obtain the Euler-Lagrange equation for non-axisymmetric drops. A second variation is then performed about an axisymmetric equilibrium solution, which results in a quadratic form in the shape perturbation $\delta f(r, \theta)$. The stability of the equilibrium solution is determined by examining whether or not this quadratic form is positive definite (stability) or can become negative for particular modes $\delta f(r, \theta)$ (instability). The quadratic form may be diagonalized in order to make this determination evident, which is accomplished by solving an associated eigenvalue problem.
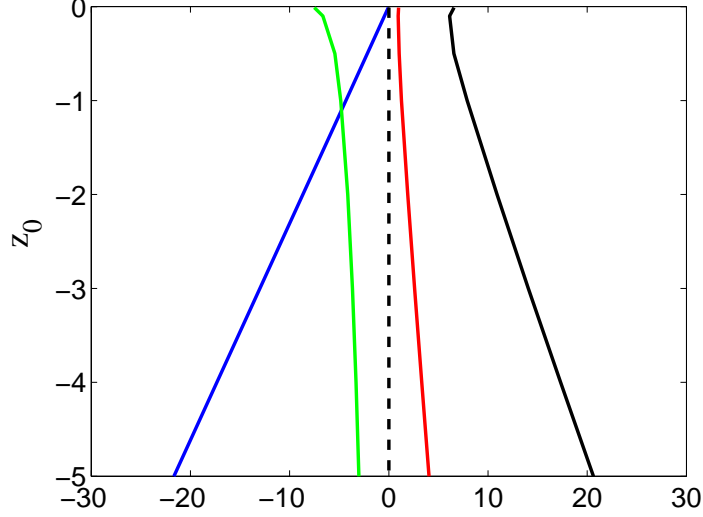
FIG. 10: Vertical force balance between the capillary forces F_0^C (blue curve) and F_1^C (red curve) at z_0 and z_1, the buoyancy force F^B (green curve), and the net constraint force due to the cone, F_T^P (black curve). Here $\alpha = 135^0$ and $\beta = 35^o$ for various drop positions z_0 (vertical axis). With these parameters drop climbs the cone with increasing Bond numbers.

A. Angle/Arclength Representation of the Second Variation

Rather than relying on the single-valued representation $r = f(z, \theta)$, it is again convenient to convert to an angle/arclength representation, in which the perturbed shape is written in the explicit form

$$\mathbf{x}(s, \theta, \epsilon) = R(s)\,\hat{r}(\theta) + Z(s)\,\hat{z} + \epsilon\,\tilde{W}(s, \theta)\,\hat{n}(s, \theta), \tag{32}$$

where $\hat{n}(s, \theta) = -Z'(s)\hat{r}(\theta) + R'(s)\hat{z}$ is the outward unit normal to the unperturbed surface, and $\epsilon\tilde{W}(s, \theta)$ is the amplitude of the perturbation, with ϵ a small expansion parameter. Since the unperturbed shape is assumed to be axisymmetric, the coefficients in the resulting equations for $\tilde{W}(s, \theta)$ are independent of θ and a Fourier representation $\tilde{W}(s, \theta) = W(s) \cos n\theta$ may be assumed. Omitting the details, the Sturm-Liouville equation that diagonalizes the second variation is given by

$$-\frac{\gamma_{LV}}{R}\frac{d}{ds}(RW_s) + \left[\frac{\gamma_{LV} n^2}{R^2}\right]W - \left[\gamma_{LV}\psi_S^2 + \gamma_{LV}\frac{\sin^2\psi}{R^2} - \Delta\rho\,g\cos\psi\right]W = \lambda\,W + \mu. \tag{33}$$

Here the eigenvalue λ should be positive (negative) for a stable (unstable) mode $W(s)$, and μ is a Lagrange multiplier for the perturbed volume constraint,

$$0 = \int_0^{2\pi}\int_0^{S_T} R(s)\,\tilde{W}(s, \theta)\,d\theta\,ds = 2\pi\delta_{n0}\int_0^{S_T} R(s)\,W(s)\,ds, \tag{34}$$

which must be enforced explicitly ($\mu \neq 0$) for axisymmetric modes ($n = 0$), but is automatically satisfied ($\mu = 0$) for non-axisymmetric modes ($n \neq 0$) due to the $\cos n\theta$ dependence of $\tilde{W}(s, \theta)$. The boundary conditions on $W(s)$ at $s = 0$ and $s = S_T$ are

$$W_s(0) - \left[\frac{\cos\alpha}{\sin\alpha}\right]\psi_s(0)W(0) = 0, \quad W_s(S_T) + \left[\frac{\cos\alpha}{\sin\alpha}\right]\psi_s(S_T)W(S_T) = 0. \tag{35}$$

Here the functions $R(s)$, $Z(s)$, and $\psi(s)$ refer to the axisymmetric unperturbed shape. The boundary condition (35) that results from the second variation is equivalent to the linearization of the Young equation (14) satisfied by the equilibrium shape, which specifies the slope of the drop at each contact line. More specifically, for a non-parametric representation $r = f(z, \epsilon)$ at a contact line $z = Z(\epsilon)$, where $f_z =$ constant, we have

$$0 = \frac{d}{d\epsilon}f_z(Z(\epsilon), \epsilon)\bigg|_{\epsilon=0} = [f_{zz}Z_\epsilon + f_{z\epsilon}]_{\epsilon=0} = f_{z\epsilon} - \left[\frac{f_{zz}}{f_z + \tan\beta}\right]f_\epsilon, \tag{36}$$
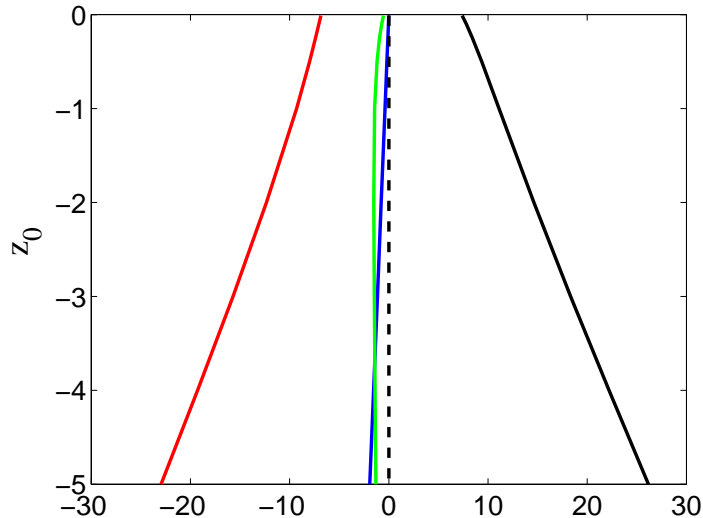
FIG. 11: Vertical force balance between the capillary forces F_0^C (blue curve) and F_1^C (red curve) at z_0 and z_1, the buoyancy force F^B (green curve), and the net constraint force due to the cone, F_T^P (black curve). Here $\alpha = 60^0$ and $\beta = 35^o$ for various drop positions z_0 (vertical axis). In this case the drop climbs the cone with increasing Bond numbers for drops that are far enough from the tip ($z_0 < -1.9$), whereas drops closer to the tip ($z_0 > -1.9$) climb the cone with decreasing Bond numbers.

where in the final expression we have used the linearization of Eq. (10), which gives $(f_z + \tan\beta)Z_\epsilon + f_\epsilon = 0$, to eliminate Z_ϵ. Converting Eq. (36) to an angle/arclength representation, and using Eq. (22), then gives (35).

1. Zero Bond Number Stability Equation

For the case of zero Bond number the Sturm-Liouville equation (33) that governs the stability of a spherical surface reduces to a Legendre differential equation [21], using $ds = R_c\,d\theta$, $R(s) = R_c\sin\theta$, and $\psi = -\theta$, where θ is a polar angle defined at the sphere center z_c.

With the boundary conditions in Eq. (35) the eigenvalue problem is still analytically intractable since the mixed boundary conditions at $s = 0$ and $s = S_T$ result in a transcendental equation for λ involving the roots of Legendre functions of the first and second kind. We have therefore implemented numerical procedures for the computation of the eigenvalues, as described below.

We note that a related problem is the stability of an isolated sphere in zero gravity, which is also described by the Sturm-Liouville equation (33) with $g = 0$. In that case, however, the appropriate boundary conditions are periodicity and regularity of $W(s)$ over the entire sphere. The sphere is neutrally stable to a lateral translation, which is represented by an $n = 1$ perturbation representing a shift in origin of the unperturbed sphere. The corresponding eigenmode is the $n = 1$ Legendre polynomial [21], $W(s) \sim P_1(\theta)$, which satisfies Eq. (33) with $n = 1$, $\mu = 0$, and $\lambda = 0$.

B. Numerical Procedures for Stability Calculations

The linear stability of an equilibrium shape is determined by computing eigenmodes $W(s)$ and eigenvalues λ from Eq. (33) with the boundary conditions in Eq. (35); if $n = 0$ the solution must be computed over the linear subspace defined by the constraint in Eq. (34). The equilibrium is stable if the eigenvalues λ are all positive, and is unstable if any eigenvalue is negative. We have used two numerical procedures for solving the constrained eigenvalue problem.

In the first procedure we use a second-order-accurate finite difference discretization of Eq. (33) in tandem with a related quadrature formula for Eq. (34) to produce a finite dimensional problem that can be solved with linear algebra software. For $n = 0$ a projection method [22] is used to handle the constraint equation, resulting in a standard matrix eigenvalue problem.
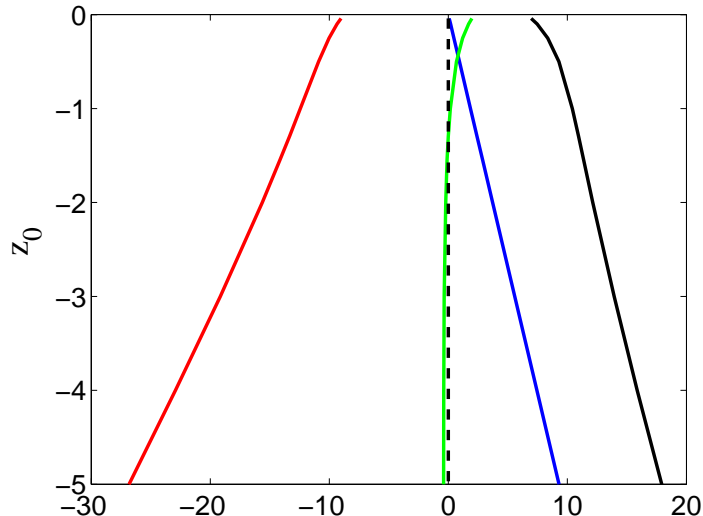
FIG. 12: Vertical force balance between the capillary forces F_0^C (blue curve) and F_1^C (red curve) at z_0 and z_1, the buoyancy force F^B (green curve), and the net constraint force due to the cone, F_T^P (black curve), for $\alpha = 30^0$ and $\beta = 35^o$ for various drop positions z_0 (vertical axis). In this case the drop climbs the cone with decreasing Bond numbers.

The second approach uses a shooting method, based on appending Eq. (33) and, for $n = 0$, the volume constraint in Eq. (34), to the system of equations used to compute the equilibrium state as described previously. The shape perturbation $W(s)$ is normalized to unity at $s = 0$, with $W_s(0)$ then set by Eq. (35). Provisional guesses for λ and (if $n = 0$) for μ are used to integrate to $s = S_T$, where the remaining boundary condition in Eq. (35) and (if $n = 0$) the volume constraint in Eq. (34) provide nonlinear equations for iteratively refining the provisional guesses. Starting guesses for λ and μ can be obtained by using the first procedure with a relatively crude mesh; the shooting procedure then gives a very accurate numerical solution based on these guesses.

C. Numerical Stability Results

We present some numerical results for a cone half-angle of $\beta = 35^o$. We first consider the case of zero Bond number, for which the drop is a section of a sphere. We then consider the general case of non-zero Bond numbers.

1. Zero Bond Number

The stability of the $Bo = 0$ solutions to $n = 1$ perturbations is shown in Fig. 13. With $\beta = 35^o$ there are $Bo = 0$ solutions for $\alpha < 55^0$; for $\alpha = 55^o$ the solution just touches the tip with $z_0 = 0$, and as α decreases the solutions move down the cone. For $n = 1$ perturbations (solid curve) that satisfy the contact condition (35) the drop is unstable ($\lambda < 0$), and the degree of instability increases with distance from the tip. For comparison, we have also included stability results for perturbations that instead satisfy a pinning condition $W = 0$ at the contact lines (dashed curves); these perturbations are found to be stable ($\lambda > 0$).

2. Non-Zero Bond Numbers

In Fig. 14 we consider a contact angle of $\alpha = 90^o$, for which the height of the drop increases monotonically with increasing Bond number. Over this range of Bond numbers the drop is unstable to axisymmetric ($n = 0$) perturbations, as indicated by the middle plot in Fig. 14. The instability becomes stronger near the tip of the cone, and tends toward neutral stability for drops farther down the cone. There are also higher $n = 0$ modes (not shown) which are found to be stable. The drop is also unstable to non-axisymmetric perturbations, as shown in the right-hand plot in Fig. 14.
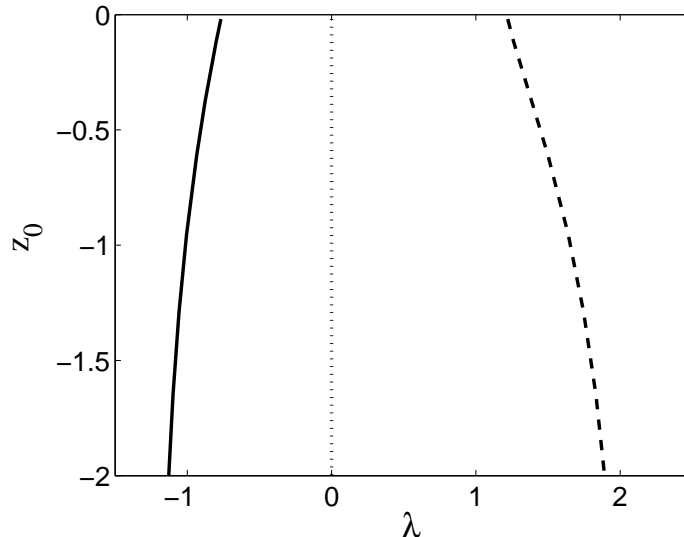
FIG. 13: Stability calculations for a conical half-angle of $\beta = 35^o$ and zero Bond numbers. The solid curve shows the stability parameter λ versus z_0 for the most dangerous $n = 1$ perturbation that satisfies the contact angle condition (35). The dashed curve shows λ versus z_0 for the most dangerous $n = 1$ perturbation that satisfies a pinned condition ($W = 0$).

The drop is always unstable to an $n = 1$ perturbation. An $n = 2$ perturbation is stable near the tip of the cone, and becomes unstable for drops farther down the cone. Again only the most dangerous modes for each n are depicted. Far enough down the cone there are instabilities to higher values of $n > 2$ as well (not shown).

In Fig. 15 we consider a contact angle of $\alpha = 30^o$, for which the height of the drop decreases monotonically with increasing Bond number. Over this range of Bond numbers the drop is stable to axisymmetric ($n = 0$) perturbations, as indicated by the middle plot in Fig. 15. The stability is stronger near the tip of the cone, and tends toward neutral stability for drops farther down the cone. The drop is unstable to non-axisymmetric perturbations, with an $n = 1$ instability that grows in strength for drops far from the tip. The $n = 2$ and $n = 3$ perturbations are stable near the tip of the cone, but become unstable for drops farther down the cone. Again only the most dangerous modes for each n are depicted. Again, far enough down the cone there are instabilities to higher values of $n > 3$ as well (not shown).

In Fig. 16 we consider an intermediate contact angle of $\alpha = 75^o$. For this value, the dependence of the height of the drop on Bo is more complicated than in the previous cases. As a function of Bond number the height of the drop is non-monotonic, and exhibits two limit points that separate regions of monotonicity, as shown by the red and blue dots in the first plot of Fig. 16. The Bond number increases with height near the cone's tip and far down the cone, and decreases with height at intermediate values. General arguments from bifurcation theory [24] show that the stability of the drop to axisymmetric perturbations changes at such limit points, as is confirmed by the $n = 0$ results in the middle plot of Fig. 16. The drops for which the height decreases with Bond number (negative slopes in Fig. 16a are found to be stable for $n = 0$ ($\lambda > 0$ in Fig. 16b, and those with positive slopes are unstable for $n = 0$, with sign changes in λ at the limit points. These findings are also consistent with the corresponding $n = 0$ results in Fig. 14 and Fig. 15, where the slopes were everywhere positive and negative, respectively. The non-axisymmetric perturbations in Fig. 16 show an $n = 1$ instability for all heights, with transitions of the $n = 2$ and $n = 3$ modes from stability to instability farther down the cone.

In Fig. 17 we consider a small contact angle of $\alpha = 15^o$. For this value, the Bond number is negative for $z_0 > -5$, and the drop is stable to axisymmetric disturbances over this range. Non-axisymmetric disturbances are also stable for $z_0 \geq -0.5581$; in particular, the $n = 1$ mode has become stable for drops close enough to the cone tip. Far enough from the tip, the $n = 1$ mode becomes unstable, as do the modes with higher value of n. Specifically, the marginal stability point for the $n = 1$ mode occurs for Bo $= -0.2721$ and $z_0 = -0.5581$. The stability with respect to $n = 1$ perturbations generally seems to occur for negative Bond numbers and relatively small values of α and β. For example, the computed stability diagrams for $(\alpha, \beta) = (30^o, 20^o)$ and $(\alpha, \beta) = (30^o, 15^o)$ (not shown) are qualitatively similar to that for $(\alpha, \beta) = (35^o, 15^o)$; specifically, we find that for $\beta = 20^o$ and $\alpha = 30^o$ the computed marginal point for the $n = 1$ mode occurs for Bo $= -0.3365$ and $z_0 = -0.4824$, and for $\beta = 20^o$ and $\alpha = 15^o$ the computed marginal point for the $n = 1$ mode occurs for Bo $= -0.1963$ and $z_0 = -1.5248$.

In all cases with positive Bond number we have found an $n = 1$ instability that generally strengthens with distance from the tip of the cone. As previously noted, an isolated sphere in zero gravity is subject to an $n = 1$ neutral mode that represents trivial translation of the sphere. The observed $n = 1$ instability of the drop resting on a cone is apparently a destabilization of this neutral mode, although the exact mechanism is difficult to understand. An example of an $n = 1$ mode near the cone tip is shown in cross-section in Fig. 18. Here the unperturbed shape is given by the blue curve, and the perturbed shape in its plane of symmetry is shown in red. The perturbation amplitude has been magnified to exaggerate the relative distortions of the contact lines nearer to and farther from the cone tip; the result is an effective tilting of the drop with respect to the horizontal. This can be compared to the tilting of drops while climbing conical substrates that are occasionally observed experimentally; see, e.g., Fig. 5c and others in Ref. ([7]).

3. Rayleigh Instability Analogy

With increasing distance from the cone tip, drops are subject to an increasing number of non-axisymmetric instabilities; only the most dangerous modes in the first three families ($n = 1, 2, 3$) of instabilities are shown in the right-most plots in Figs. 13-16. For drops that are far removed from the tip, an interpretation of these high-wavenumber modes is possible in terms of a classical surface-tension-driven instability. For example if we consider contact angles $\alpha \geq 90^o$ the cross section of the drops become more and more circular for drops that are far from the cone tip as the Bond number becomes small (c.f. Fig. 4), and the drops resemble half of a torus that is bisected by the cone. For large values of the effective major radius of the drop, the non-axisymmetric instabilities are then analogous to the capillary-driven Rayleigh instabilities [23] of an equivalent cylinder of length $2\pi R_M$ and radius r_m, where R_M and $r_m \ll R_M$ are the major and minor radii of the torus. The onset of the Rayleigh instability occurs for a perturbation whose wavelength λ_R is equal to the circumference $2\pi r_m$ of the cylinder [23]. For an effective cylinder length $L = 2\pi R_M$ we therefore anticipate neutral modes with mode number n_R such that $n_R \lambda_R = L$, or $n_R = R_M/r_m$. We can readily compute values for R_M and r_m from the numerical solution in this regime (which satisfy $R_M + z_0 \tan \beta \approx 0$ and $(2\pi R_M)(\pi r_m^2) \approx V_D$) and compare this estimate for n_R with the numerically-computed values of n that have crossings at $\lambda_n = 0$. For example, in Fig. 14 the $n = 3$ mode with $z_0 = -1.29$ is neutrally stable ($\lambda_3 = 0$). For this drop, the computed radii are $R_M = 1.2403$ and $r_m = 0.5817$, which gives the estimate $n_R = 2.13$. The estimate becomes more accurate for drops with larger values of R_M; for a drop with $z_0 = -20.02$ we find $R_M = 14.1176$ and $r_m = 0.1734$, giving $n_R = 81.42$. The corresponding numerical results show that the perturbation with $n = 82$ is neutrally stable under these conditions. Some numerical results are summarized in Table I. The analytical approximation may also be obtained directly from the Jacobi equation (33) in this regime: the dominant balance for $\lambda = 0$ is found to be

$$\frac{\gamma_{LV} n^2}{R^2} W \approx \gamma_{LV} \psi_s^2 W, \quad W_s(0) = W_s(S_T) = 0, \tag{37}$$

where for the semi-circular base state we have $R(s) \approx R_M$, $S_T \approx \pi r_m$ and $\psi_s \approx 1/r_m$. The resulting eigenmode $W(s)$ is approximately constant, with $n^2 = R_M^2/r_m^2$ as in Rayleigh's analysis.

Table I: Large n neutral modes for $\beta = 35^o$ and $\alpha = 90^o$.

Bo	z_0	R_M	r_m	$n_R = R_M/r_m$	$n(\lambda_n = 0)$
0.730648	-1.29478	1.24026	0.581686	2.132	3
0.688197	-1.91825	1.63465	0.508187	3.217	4
0.516970	-5.15074	3.79834	0.334305	11.362	12
0.391414	-10.0255	7.15959	0.243514	29.401	30
0.283351	-20.0200	14.1176	0.173400	81.416	82

VI. DISCUSSION

We have considered the equilibrium and stability of axisymmetric drops that rest on the side of a conical substrate, motivated by experimental observations of the dynamics of cellular clusters. The results for both equilibrium and stability in the fluid model presented here are more complicated than we originally anticipated; it would be useful to have experimental validations for some of the predicted behavior in this simpler case. In our solution procedure we have generally prescribed the conical half-angle β, the contact angle α, and the drop height z_0, and computed the
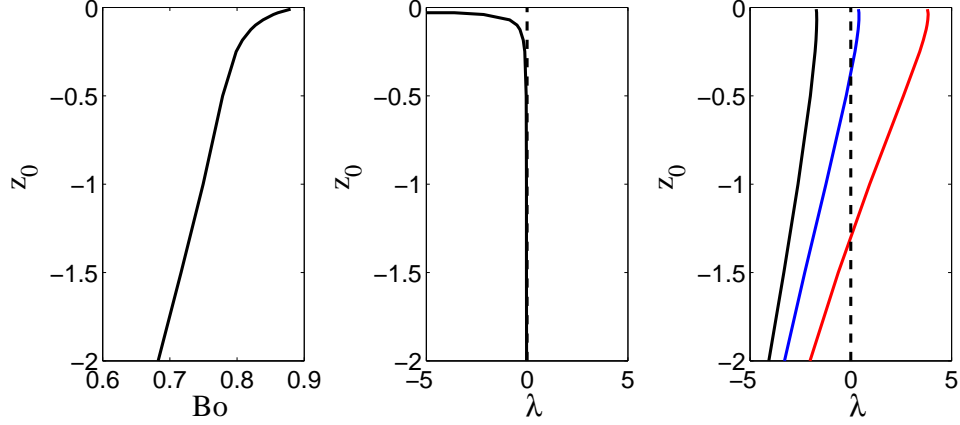
FIG. 14: Stability calculations for a conical half-angle of $\beta = 35^o$ and a contact angle of $\alpha = 90^o$. The left hand plot shows the position, z_0, of the upper contact line of the equilibrium drop as a function of the Bond number, Bo. The middle plot shows the most dangerous axisymmetric stability eigenvalue, λ, as a corresponding function of z_0; the drops are unstable ($\lambda < 0$) to axisymmetric disturbances over this range of Bo. The right hand plot shows the lowest non-axisymmetric modes for $n = 1$ (black curve), 2 (blue curve), and 3 (red curve) as a function of z_0.
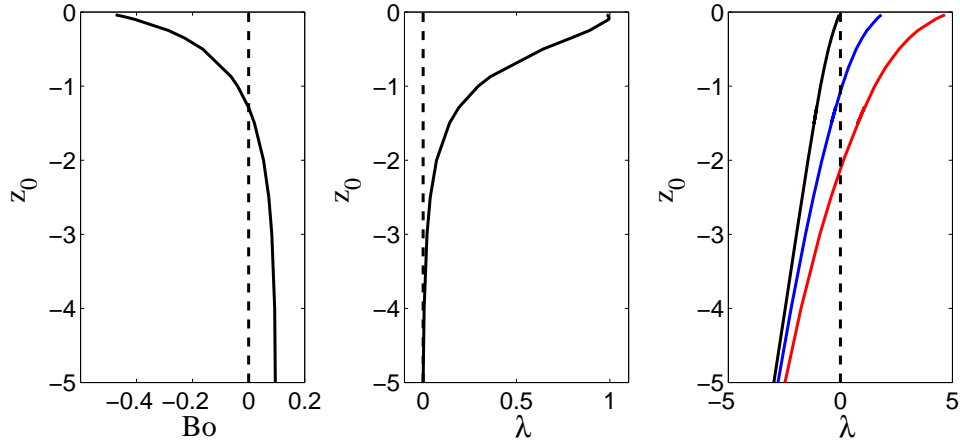
FIG. 15: Stability calculations for a conical half-angle of $\beta = 35^o$ and a contact angle of $\alpha = 30^o$. The left hand plot shows the position, z_0, of the upper contact line of the equilibrium drop as a function of the Bond number, Bo. The middle plot shows the most dangerous axisymmetric stability eigenvalue, λ, as a corresponding function of z_0; the drops are stable ($\lambda > 0$) to axisymmetric disturbances over this range of Bo. The right hand plot shows the lowest non-axisymmetric modes for $n = 1$ (black curve), 2 (blue curve), and 3 (red curve) as a function of z_0.

corresponding Bond number and drop shape; equilibria for either upward-pointing cones (corresponding to positive Bond numbers Bo) or for downward-pointing cones (negative Bond numbers) are then obtained depending on the sign of the Bond number. As seen in Fig. 12, the force balance for solutions with Bo < 0 is primarily between the capillary forces and the forces of constraint, with the buoyancy contribution playing a minor role.

Considered as a one parameter family of solutions with changing height z_0 and Bond number Bo for fixed values of α and β, the solution branches can exhibit one or more limit points where the number of solutions changes as Bo varies (cf. Fig. 16). At such limit points, general arguments [24] predict that the limit point is a point of marginal stability to axisymmetric perturbations, and this is borne out in the numerical calculations. The determination of the stability of the solutions to axisymmetric perturbations is thus largely characterized by the geometrical shape of the solution branches. Based on numerical simulations we generally find that solutions with large values of β and α tend
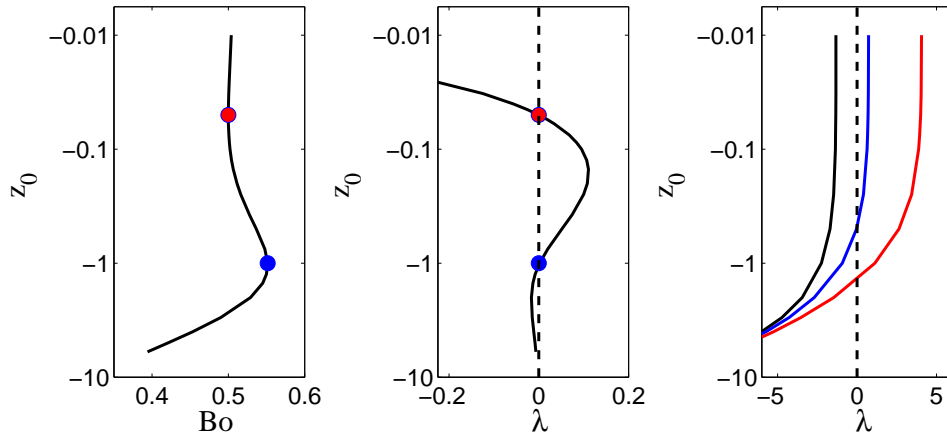
FIG. 16: Stability calculations for a conical half-angle of $\beta = 35^o$ and a contact angle of $\alpha = 75^o$. The left hand plot shows the position, z_0, of the upper contact line of the equilibrium drop as a function of the Bond number, Bo. Two limit points where the slope of the curve changes sign are indicated by the red and blue dots. The middle plot shows the most dangerous axisymmetric stability eigenvalue, λ, as a corresponding function of z_0. The drops are stable ($\lambda > 0$) to axisymmetric disturbances for values of z_0 that lie between the two limit points, with marginal stability ($\lambda = 0$) at these limit points. The right hand plot shows the lowest non-axisymmetric modes for $n = 1$ (black curve), 2 (blue curve), and 3 (red curve) as a function of z_0.

to have positive Bond numbers and to be unstable to axisymmetric perturbations. Solutions with small values of β and α tend to be stable to axisymmetric perturbations, at least for drops that are not too far from the tip. Solutions with small enough contact angles tend to correspond to negative Bond numbers. For intermediate values of α and β there can be multiple solutions for a given Bond number, with differing stability to axisymmetric perturbations.

The stability of the solutions to non-axisymmetric perturbations generally requires a separate calculation of the second variation of the energy functional. We have found a range of completely stable solutions that are characterized by negative Bond numbers and small values of α and β (see Fig. 17); these solutions are located near the cone tip, and become unstable to non-axisymmetric perturbations for drops far from the tip. We find that solutions with positive Bond number are frequently unstable to non-axisymmetric perturbations. Drops that are far from the tip tend to be unstable to several non-axisymmetric modes; these instabilities resemble the classical Rayleigh instability of a cylinder. Drops near the cone tip tend to be stable to higher order modes of non-axisymmetric perturbations, but for positive Bond numbers an instability to $n = 1$ perturbations persists.

For an isolated spherical equilibrium with Bo $= 0$, such $n = 1$ perturbations correspond to neutrally-stable translations of the sphere. For equilibrium drops on a cone with Bo $= 0$, these $n = 1$ perturbations are apparently destabilized by the contact angle boundary condition which fixes the slope of the drop at the contact line. If the contact condition is replaced by a pinning condition that instead fixes the location of the contact line the $Bo = 0$ drops are found to be stable to $n = 1$ perturbations. A limited number of numerical calculations (not shown) with non-zero Bond numbers indicate that the drops are less unstable to $n = 1$ perturbations with pinned boundary conditions than they are to contact angle conditions. We also note that with our contact angle conditions we have found axisymmetric equilibrium shapes that are stable to axisymmetric perturbations but unstable to non-axisymmetric perturbations. It is known [25] that for single-valued [i.e., $r = f(z)$] axisymmetric equilibrium shapes with pinned boundary conditions, if the shape is stable to axisymmetric perturbations, it is then also stable to non-axisymmetric perturbations as well.

It is interesting to contrast the case of drops on a conical substrate with the case of drops on a vertical cylinder. In zero gravity (Bo $= 0$) there are solutions for either case for small enough contact angles α, and the drops are sections of a punctured sphere. In the cylindrical case, there are also non-spherical solutions for large enough values of α (see Fig. 8). In the conical case, we find no non-spherical Bo $= 0$ solutions; if we start with a spherical solution on the cone and increase α the drop will climb the cone (remaining spherical) until the upper contact line reaches the tip, with an associated contact angle of $\alpha = \pi/2 - \beta$. On the other hand, with a gravitational field, say with Bo > 0, there are no equilibrium drops on a smooth cylinder that satisfy the contact angle condition: if there were such a solution, a rigid downward translation of the drop would decrease the energy of the solution so it cannot represent a stationary state.

We note that stationary drops on a vertical surface with Bo $\neq 0$ can be observed in the presence of surface defects
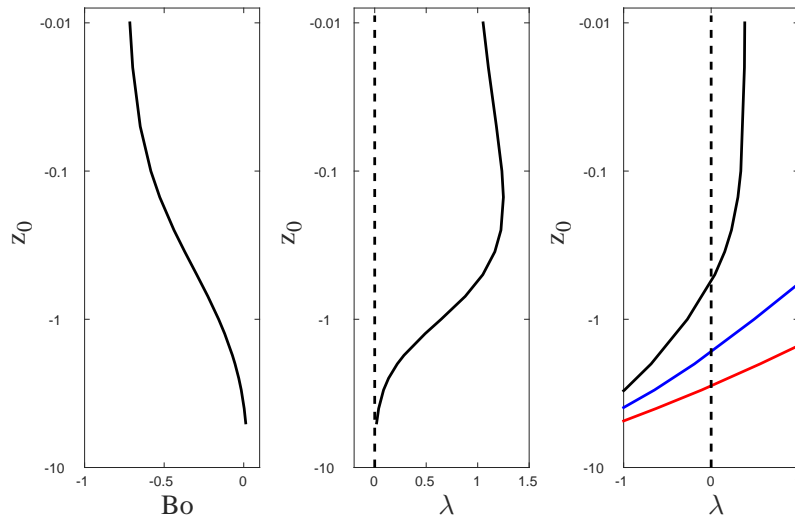
FIG. 17: Stability calculations for a conical half-angle of $\beta = 35^o$ and a contact angle of $\alpha = 15^o$. The left hand plot shows the position, z_0, of the upper contact line of the equilibrium drop as a function of the Bond number, Bo. The middle plot shows the most dangerous axisymmetric stability eigenvalue, λ, as a corresponding function of z_0. The drops are stable ($\lambda > 0$) to axisymmetric disturbances for all values of z_0 in this range. The right hand plot shows the lowest non-axisymmetric modes for $n = 1$ (black curve), 2 (blue curve), and 3 (red curve) as a function of z_0. The drops are stable to non-axisymmetric disturbances for $z_0 > -0.5$.

such as localized roughness, contaminants, or other inhomogeneities, which can effectively pin the contact line; in these circumstances hysteresis of observed contact angles is possible [26]. The variation of the contact line position that is used in the derivation of the Young equilibrium condition (14) in our treatment is then ruled out, resulting in a more complicated model for drop equilibrium and stability than we have considered here.

The equilibrium drops on a cone with Bo $\neq 0$ that are found under suitable conditions have complicated limiting behavior in the limit of small β, either tending to climb to the tip or descend to infinity with variations in β. We note that there are solution branches for fixed α and β that have Bo $\to 0$ and $z_1 \to -\infty$, which tend to resemble sections of a torus; here the value of the Lagrange multiplier $P \to 0$ as well, meaning that the solutions are tending to zero mean curvature in this limit.

A drop nearing the tip of the cone eventually is not well-described by the model as the upper contact line contracts to a point. A model in which the cone tip lies in the interior of the drop, with a single contact line at $z = z_1$, would be a straightforward modification of the current treatment. This model might be relevant to studies of the vapor-liquid-solid (VLS) geometry in the growth of nanowires [27].

VII. ACKNOWLEDGMENTS

[1] Pierre-Gilles de Gennes, Francoise Brochard-Wyart, and David Quere, Capillarity and Wetting Phenomena: Drops, Bubbles, Pearls, Waves (Springer, Berlin, 2004).

[2] H.M. Princen, "The equilibrium shape of interfaces, drops, and bubbles. Rigid and Deformable particles at interfaces," in Surface and Colloid Science, Vol. 2, ed. Egon Matijevíc, (Wiley-Interscience, New York, 1969), pp.1–84.

[3] D.H. Michael, "Meniscus Stability," Annual Review of Fluid Mechanics **81**, 189–215 (1981).
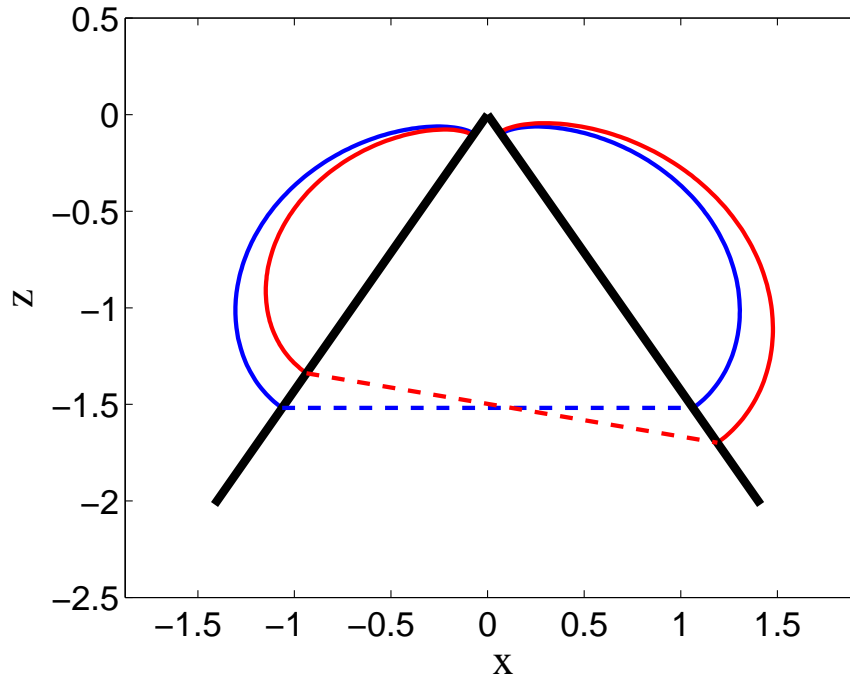
FIG. 18: An equilibrium shape (in blue) that is unstable to an $n = 1$ perturbation for a conical half-angle of $\beta = 35^o$ and a contact angle of $\alpha = 90^o$ with Bond number Bo = 0.828. The resulting perturbed shape (in red) is shown with an exaggerated perturbation amplitude for visual purposes.

[4] A.J.B. Milne, B. Defez Garcia, M.A. Cabrerizo-Vílchez, and A. Amirfazli, "Understanding (sessile/constrained) bubble and drop oscillations," Adv. Colloid Interface Sci. **203**, 22–36 (2014).

[5] J.B. Bostwick and P.H. Steen, "Stability of constrained capillary surfaces," Annual Review of Fluid Mechanics **47**, 539–68 (2015).

[6] A. Nurse, L. B. Freund, and J. Youssef, "A Model of Force Generation in a Three-Dimensional Toroidal Cluster of Cells," Journal of Applied Mechanics **79**, 051013 (2012).

[7] J. Youssef, A.K. Nurse, L. B. Freund, and J.R. Morgan, "Quantification of the forces driving self-assembly of three-dimensional microtissues," Proceedings of the National Academy of Sciences **108**, 6993–6998 (2011).

[8] S.R. Coriell and M.R. Cordes, "Theory of molten zone shape and stability," J. Crys. Growth **42**, 466–472 (1977).

[9] E. Pairam and A. Fernández-Nieves, Generation and stability of toroidal droplets in a viscous liquid, Phys. Rev. Lett. **102**, 234501 (2009).

[10] J.D. McGraw, J. Li, D.L. Tran, A.C. Shi and K. Dalnoki-Veress, Plateau-Rayleigh instability in a torus: formation and breakup of a polymer ring, Soft Matter **6**, 1258–1262 (2010) .

[11] Y. Wu, J.D. Fowlkes, P.D. Rack, J.A. Diez, and L. Kondic, On the breakup of patterned nanoscale copper rings into droplets via pulsed-laser-induced dewetting: competing liquid-phase instability and transport mechanisms. Langmuir **26**, 11972–11979 (2010).

[12] J.B. Bostwick and P.H. Steen, "Stability of constrained cylindrical interfaces and the torus lift of PlateauRayleigh," J. Fluid Mech. **647** 201–219 (2010).

[13] A.G. González, J.A. Diez, and L. Kondic, "Stability of a liquid ring on a substrate," Journal of Fluid Mechanics **718**, 246–279 (2013).

[14] Z. Yao and M.J. Bowick, The shrinking instability of toroidal liquid droplets in the Stokes flow regime, Eur. Phys. J. E **34**, 32 (2011).

[15] S. Zhao and J. Tao, Instability of a rotating liquid ring, Phys. Rev. E **88**, 033016 (2013).

[16] H. Mehrabian and J.J. Feng, Capillary breakup of a liquid torus, J. Fluid Mech. **717**, 281–292 (2013).

[17] T.D. Nguyen, M. Fuentes-Cabrera, J.D. Fowlkes, J.A. Diez, A.G. Gonzlez, L. Kondic, and P.D. Rack, Competition between collapse and breakup in nanometer-sized thin rings using molecular dynamics and continuum modeling, Langmuir **28**, 13960–13967 (2012).

[18] B.D. Texier, K. Piroird, D. Qur, and C. Clanet, Inertial collapse of liquid rings, J. Fluid Mech. **717**, R3-1 – R3-10 (2013).

[19] S.H. Davis, Theory of Solidification (Cambridge University Press, Cambridge, UK, 2001).

[20] F. Julicher and U. Seifert, "Shape equations for axisymmetric vesicles: A clarification," Physical Review E **49**, 4728–4731 (1994).

[21] NIST Handbook of Mathematical Functions, ed. Frank W. J. Olver, Daniel W. Lozier, Ronald F. Boisvert, and Charles W. Clark, (Cambridge University Press, New York, 2010).

[22] G.H. Golub, "Some modified matrix eigenvalue problems," SIAM Review **15**, 318–334 (1973).

[23] P.G. Drazin and W.H. Reid, Hydrodynamic Stability (Cambridge University Press, New York, 1981).

[24] G. Ioss and D.D. Joseph, Elementary Stability and Bifurcation Theory (Springer, New York, 1980).

[25] R.D. Gillette and D.C. Dyson, "Stability of axisymmetric liquid-fluid interfaces towards general disturbances," The Chemical Engineering Journal **3**, 196–199 (1972).

[26] P.G. DeGennes, "Wetting: statics and dynamics," Rev. Mod. Phys. **57**, 827–863 (1985).

[27] E.J. Schwalbach, S.H. Davis, P.W. Voorhees, J.A. Warren, and D. Wheeler, "Stability and topological transformations of liquid droplets on vapor-liquid-solid nanowires," J. Appl. Phys. **111**, 024302 (2012).